Ceramics International xxx (xxxx) xxx

Contents lists available at ScienceDirect

Ceramics International

journal homepage: www.elsevier.com/locate/ceramint

Porous agarose/Gd-hydroxyapatite composite bone fillers with promoted osteogenesis and antibacterial activity

Chunling Yang [a,b], Qianhong Ren [b,d], Xiaomei Liu [b], Yi Liu [b,c,**], Botao Zhang [b], Ping Zhou [b], Hua Li [b,c,*]

[a] Henan Institute of Advanced Technology, Zhengzhou University, Zhengzhou, 450052, China
[b] Zhejiang Engineering Research Center for Biomedical Materials, Cixi Institute of Biomedical Engineering, Ningbo Institute of Materials Technology and Engineering, Chinese Academy of Sciences, Ningbo, 315201, China
[c] Institute of Applied Physics, Jiangxi Academy of Sciences, Nanchang, 330029, China
[d] State Key Laboratory of Advanced Special Steel, School of Materials Science and Engineering, Shanghai University, Shanghai, 200444, China

ARTICLE INFO

Keywords:
Agarose/gd-HA fillers
Antibacterial property
Biocompatibility
Three-dimensional structure

ABSTRACT

Artificial bone fillers are essentially required for repairing bone defects, and developing the fillers with synergistic biocompatibility and anti-bacterial activity persists as one of the critical challenges. In this work, a new agarose/gadolinium-doped hydroxyapatite filler with three-dimensional porous structures was fabricated. For the composite filler, agarose provides three-dimensional skeleton and endows porosity, workability, and high specific surface area, hydroxyapatite (HA) offers the biocompatibility, and the rare earth element gadolinium (Gd) acts as the antibacterial agent. X-ray photoelectron spectroscopy detection showed the doping of Gd in HA lattice with the formation of Gd-HA interstitial solid solution. Attenuated total reflection Fourier transform infrared spectroscopy imaging suggested chemical interactions between agarose and Gd-HA, and the physical structure of agarose was tuned by the Gd-doped HA. Cytotoxicity testing and alizarin red staining experiments using mouse pro-osteoblasts (MC3T3-E1) revealed remarkable bioactivity and osteogenic properties of the composite fillers, and proliferation and growth rates of the cells increased in proportion to Gd content in the composites. Antibacterial testing using the gram-positive bacteria *S. aureus* and the gram-negative bacteria *E. coli* indicated promising antibacterial properties of the fillers. Meanwhile, the antibacterial properties of composite filles were enhanced with the increase of Gd content. The antibacterial fillers with porous structure and excellent physicomechanical properties show inspiring potential for bone defect repair.

1. Introduction

Orthopedic disease and bone defects, such as osteoporosis that occurs with aging or bone loss caused by accidents, have been common for decades [1,2], demanding the development of bone repair and bone implantation techniques [3]. A variety of biomaterials have been proposed, such as medical bioceramics [4], medical polymers [5], medical composites [6], and nano-artificial bone [7]. For ideal bone implant materials, appropriate bioactivity to promote bone and tissue regeneration, essential antibacterial ability to resist bacterial infections, and adequate mechanical strength are all required [8]. Therefore, extensive research efforts have been devoted to developing or modifying bone implant materials to meet these requirements or improve their properties.

Among the biomaterials developed so far, due to their porous three-dimensional structure and high specific surface area, hydrogel material favors the storage of human body extracellular matrix that can stimulate cell growth and is conducive to cell migration [9,10]. Various hydrogel materials such as chitosan [11], agarose [12], and polylactic acid [13] have been studied for biomedical applications. Agarose, a biocompatible and biodegradable natural polysaccharide extracted from the purplish red seaweed, is commonly applied in biology and pharmacy [14]. It has

* Corresponding author. Zhejiang Engineering Research Center for Biomedical Materials, Cixi Institute of Biomedical Engineering, Ningbo Institute of Materials Technology and Engineering, Chinese Academy of Sciences, Ningbo, 315201, China.
** Corresponding author. Zhejiang Engineering Research Center for Biomedical Materials, Cixi Institute of Biomedical Engineering, Ningbo Institute of Materials Technology and Engineering, Chinese Academy of Sciences, Ningbo, 315201, China
E-mail addresses: liuyi@nimte.ac.cn (Y. Liu), lihua@nimte.ac.cn (H. Li).

https://doi.org/10.1016/j.ceramint.2021.12.137
Received 6 October 2021; Received in revised form 7 December 2021; Accepted 13 December 2021
Available online 17 December 2021

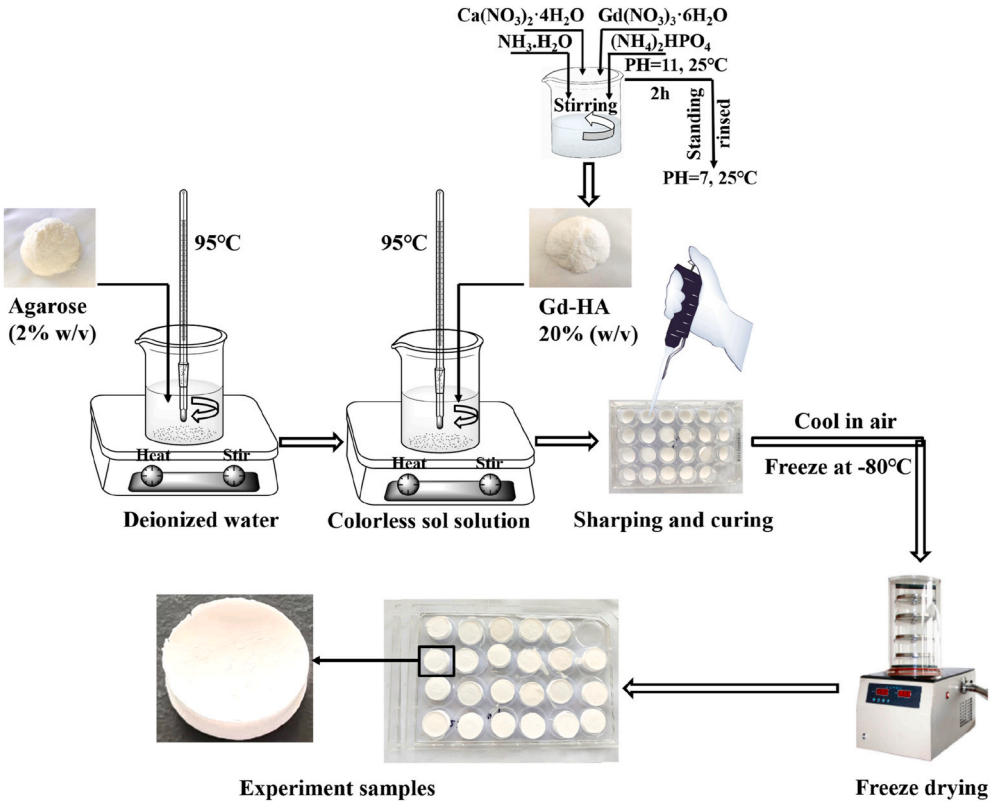

Fig. 1. Schematic depiction of the sample preparation procedures.

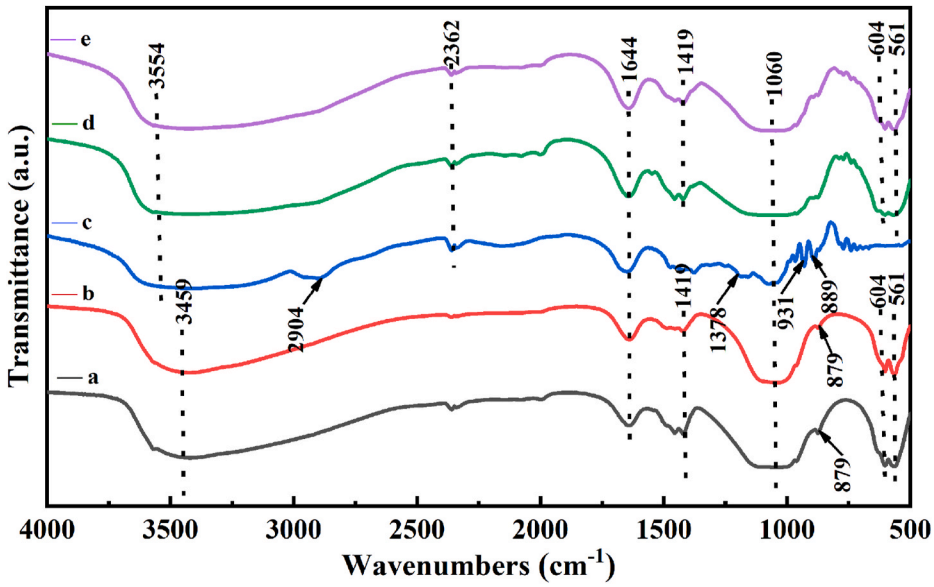

Fig. 2. ATR-FTIR spectra of the samples, a: HA, b: $Gd_{0.1}$-HA, c: agarose, d: agarose-HA, and e: agarose-$Gd_{0.1}$-HA.

been widely studied in bone tissue engineering due to its excellent biocompatibility, no immune rejection reaction and high workability. In particular, agarose with three-dimensional structure can both facilitate cell adhesion, migration and provide support for the creation of an environment for extracellular matrix [15,16]. The irregularity of bone defects demands changeable shape of the fillers and the good machinability of agarose makes it a good candidate as the potential bone defect filler [17,18]. However, previous studies have shown that pure agarose did not perform well for cell adhesion and its mechanical properties are poor [19], hence it is often used as one of the components for making composite structures, for instance chitosan-agarose [20], mussel-agarose composite [21], hydroxyapatite (HA)-agarose [22].

As one of the natural components of human bone tissues [23,24], HA possesses excellent biocompatibility and similar mechanical properties with bone, which make it suitable as bone filling and bone supporting material [25]. HA is usually used alone as bone fillers or as an additive to improve the biocompatibility of materials in the bone engineering [26,27]. Regardless of the capability of HA to provide stiff support to damaged hard bone and facilitate new bone growth on its surface, HA lacks the biological performance that is required to build a biological

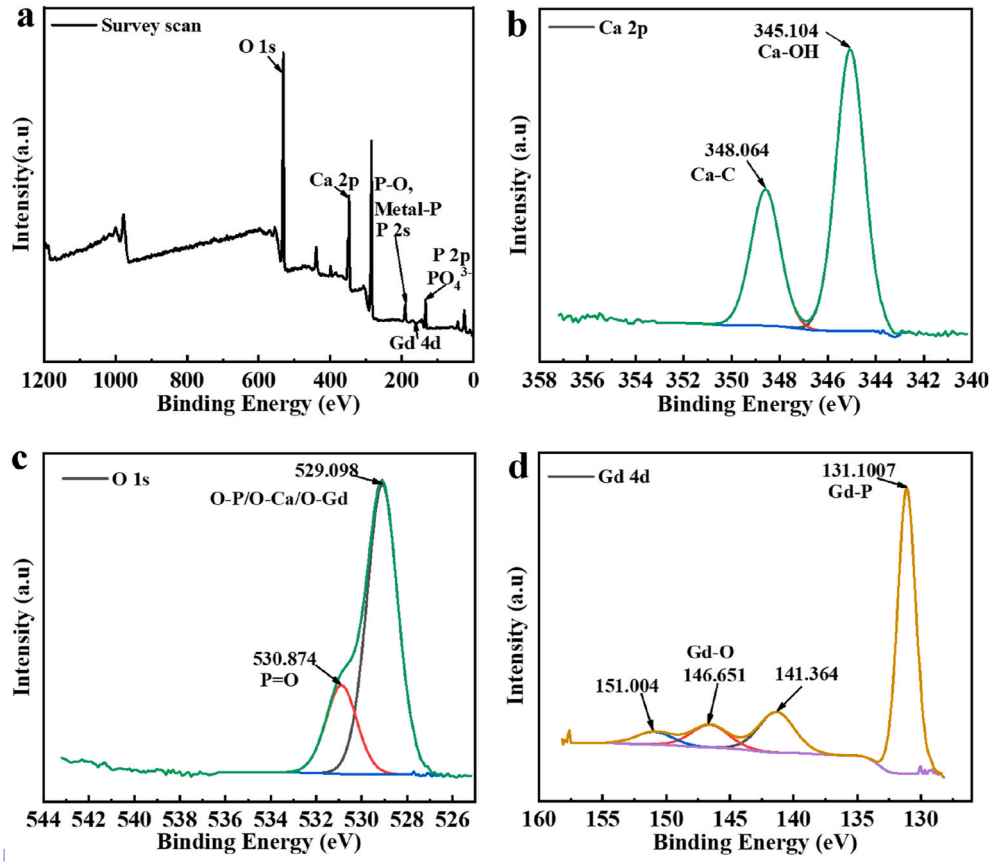

Fig. 3. XPS survey scan of the $Gd_{0.1}$-HA sample (a), and XPS narrow scans of Ca 2p (b), O 1s (c), and Gd 4d (d).

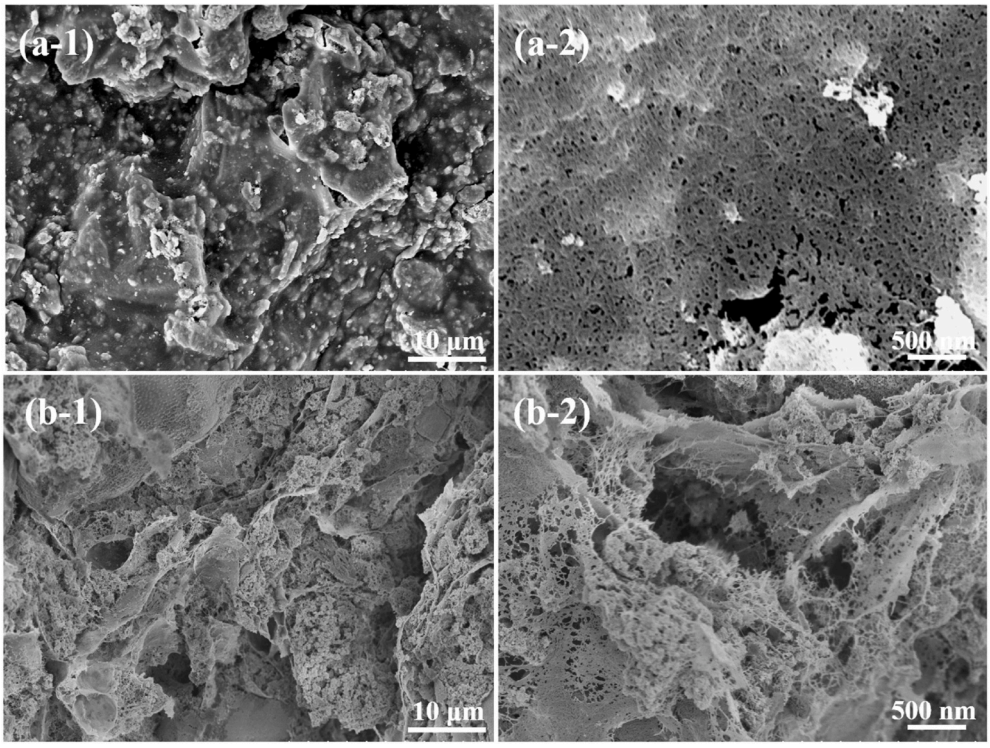

Fig. 4. SEM images showing the topographical and cross-sectional morphology of the agarose-HA sample, a: surface morphology, and b: cross-sectional morphology (−1: low magnification view, −2: magnified view).

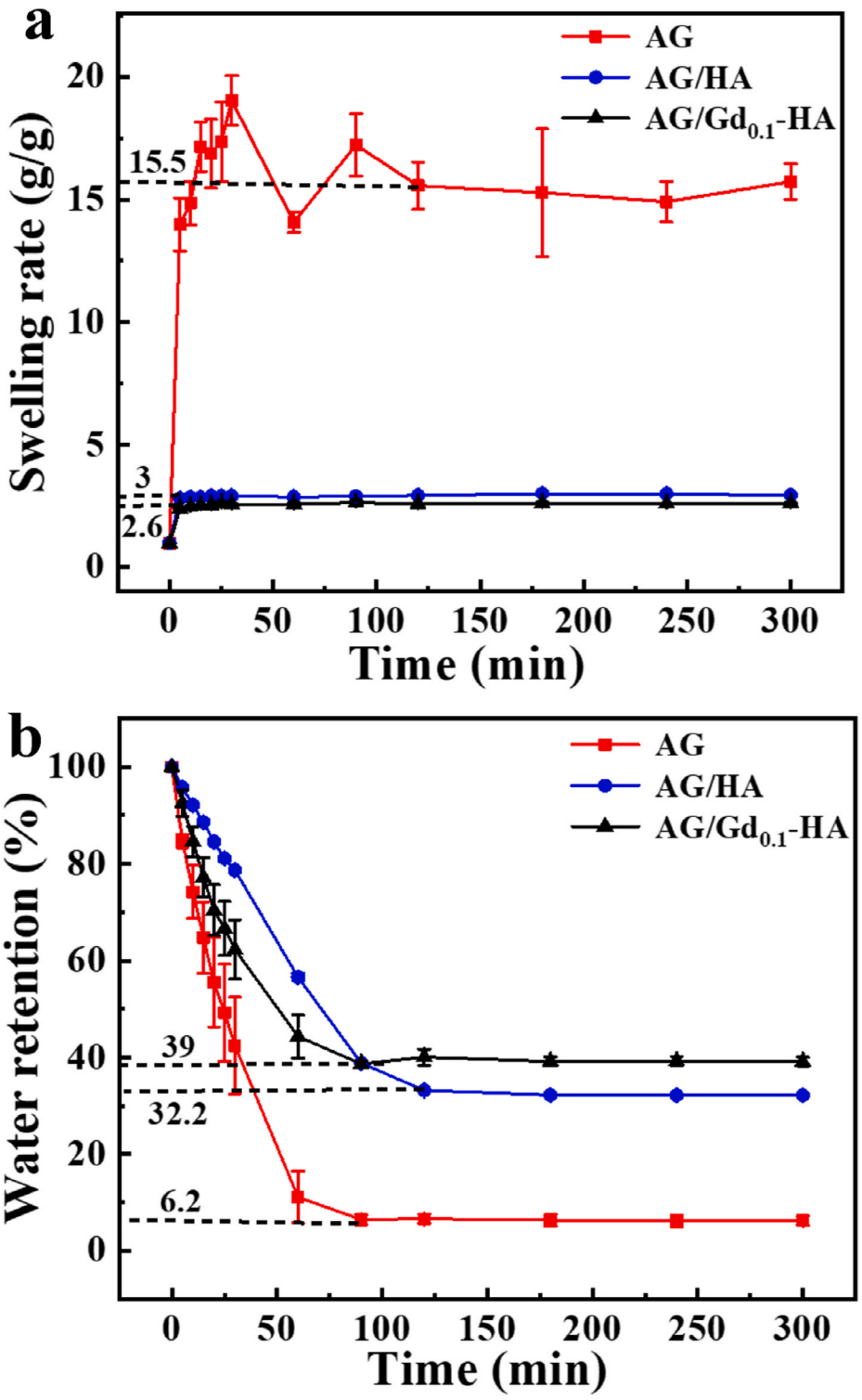

Fig. 5. Swelling ratio (a) and water retention (b) of the agarose, the agarose-HA, the agarose/$Gd_{0.1}$-HA fillers. AG stands for agarose.

function with bone tissue [28]. Besides, HA intrinsically has no antibacterial activities, therefore, it is unable to cope with the bacterial infection problem, which greatly reduces the surgical success rate and the service life of the implant [29]. To improve the biological function of HA, compound of HA/SiO_2 and synthesizing HA derivatives such as TCP, CPS have been reported [30,31]. Studies on the antibacterial modification of HA mainly involved lattice modification of HA like doping of antibacterial silver ions, copper/cuprous ions, zinc ions, ferric ions, and others [32,33], or incorporation of antibacterial phases like TiO_2, nano-Ag particles and other materials to make HA-based composites [34].

Gadolinium (Gd) is one of the rare earth elements and a sort of trace element in human bone, it possesses certain biological properties including sterilization and anti-inflammatory function, and low toxicity [35]. As a relatively new antibacterial agent, it has been studied by many researchers [36]. As reported, Gd owns favorable antibacterial effects against both gram-negative bacteria and gram-positive ones, together with good biocompatibility. According to a previous study,

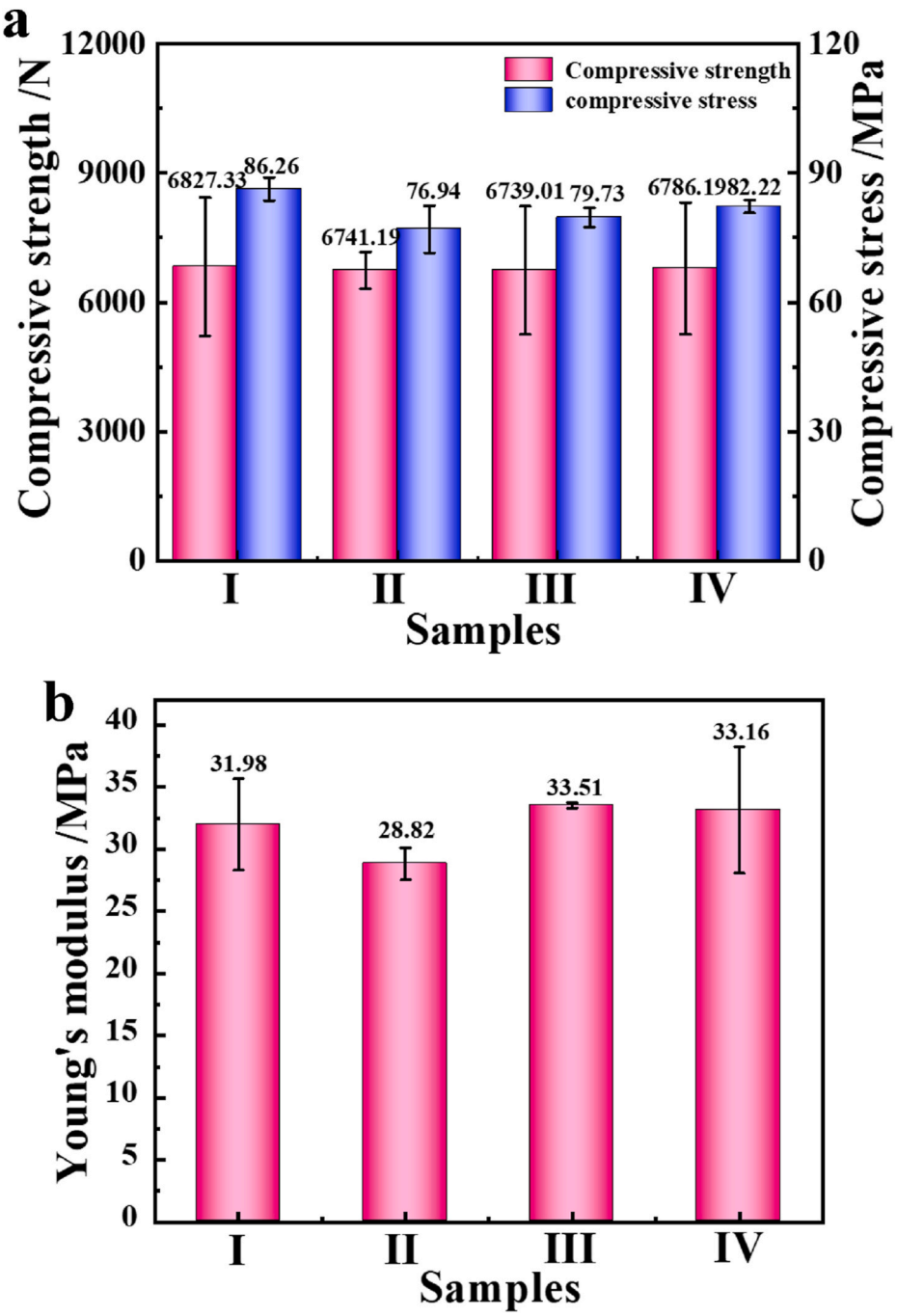

Fig. 6. Mechanical properties of the samples, a: compress strength and compressive stress, and b: Young's modulus (I: agarose/HA, II: agarose/$Gd_{0.05}$-HA, III: agarose/$Gd_{0.075}$-HA, IV: agarose/$Gd_{0.1}$-HA).

Gd^{3+} can be doped in HA by replacing Ca^{2+} [37]. This work focused on the preparation and characterization of biocompatible agarose/Gd-HA composites with antibacterial performances for bio-fillers applications. In the newly designed structure, agarose was used as the basic skeleton, Gd-doped HA played as the bio-phase. Excellent antibacterial performance, biological activity and mechanical properties were achieved through the excellent biocompatibility of HA and the characteristics of Gd that can sterilize and promote cell growth. For the agarose/Gd-HA fillers, three-dimensional structure with large specific surface area was constructed. The structural features make it easy to create suitable environment for tissue ingrowth and cell contact. Moreover, excellent workability of the structure offers the ease for the fillers to be used in various environments.

2. Materials and methods

2.1. Preparation of Gd-HA powder and agarose/Gd-HA fillers

Gd-doped HA (Gd-HA) powder was synthesized through chemical precipitation following the protocol reported previously [38]. The atomic ratio ($Gd^{3+}/(Ca^{2+}+Gd^{3+})$) was 0.05, 0.075, and 0.1, respectively. They were denoted as Gd_x-HA (x = 0.05, 0.075, 0.1). Agarose/Gd-HA fillers with 2% w/v agarose and 20% w/v Gd-HA were prepared. To make the fillers, a colorless and transparent gel solution was prepared by stirring 2 g of agarose (Aladdin, China) in 100 mL deionized water at 95 °C. Then 20 g of Gd-HA powder was added to the gel solution, and the suspension was stirred until it became uniform and

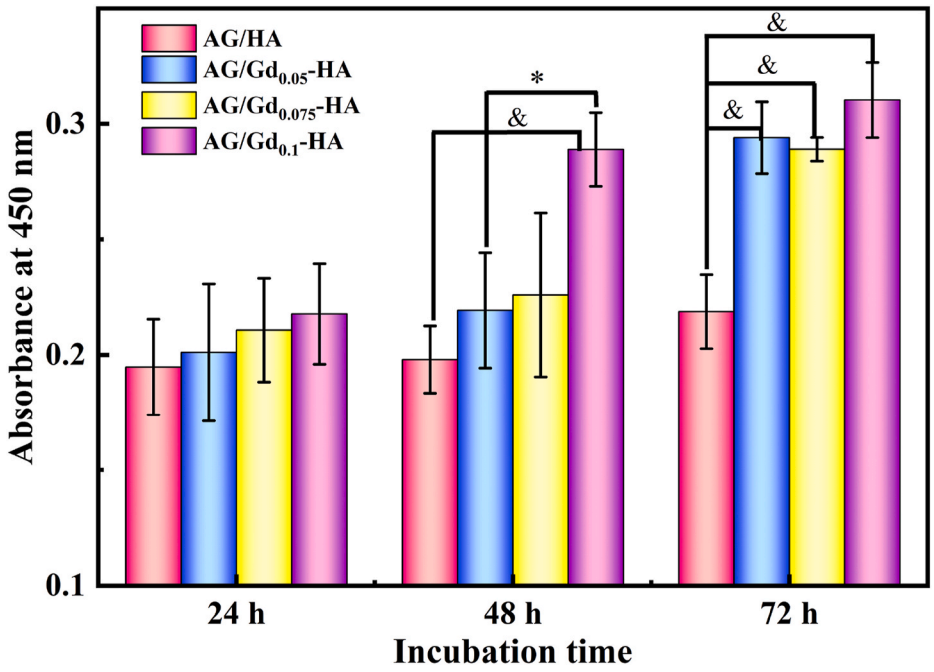

Fig. 7. Cell proliferation assay examination after the culturing of 24 h, 48 h, 72 h $^{*}P < 0.05$, $^{\&}P < 0.005$.

white. Subsequently, the suspension was transferred to 24-well plate with 500 μL for each well, followed by air-cooling and pre-freezing in refrigerator at −80 °C, and final drying by a freeze-dryer (ALPHA 1–4 LD plus, Christ, Germany). The sample preparation is schematically shown in Fig. 1.

2.2. Sample characterization

Chemistry of the prepared Gd-HA was examined by X-ray photoelectron spectroscopy (XPS, AXIS SUPRA, Kratos, England). Attenuated total reflection Fourier transform infrared spectroscopy imaging (ATR-FITR, Nicolet iS50, Thermo Scientific, America) was employed to analyze the functional groups of the agarose, HA, Gd-HA, agarose/Gd-HA samples and characterize the interactions between different phases. The surface and internal morphologies of agarose/Gd-HA fillers were examined by scanning electron microscopy (SEM, Regulus 8230, Hitachi, Japan).

Swelling rate (*SR*) of the samples was examined. Weight of the freeze-dried samples was recorded (W_0), and each of the samples was soaked in PBS at 25 °C. The sample was taken out, wiped, and weighed (W_t) for every interval (5 min for the first 30 min, 30 min for the next 90 min, and 1 h for the first 2 h), until the difference of the sample weight to the last weighing was less than 0.01 g. The *SRs* at different time interval were calculated according to the following formula:

$$SR = W_t/W_0 \quad (1)$$

Water retention experiment was also carried out. Firstly, the sample reached adsorption equilibrium in PBS at 25 °C, and the weight was recorded as W_0. Then these samples were transferred to 37 °C air-drying oven, and the weight at each interval (the same as the swelling rate testing) was recorded as W_t. The water retention rate (*WR*) was defined as per the following equation:

$$WR\ (\%) = (W_t/W_0) \times 100\% \quad (2)$$

Mechanical properties of the filles (the samples with 19 mm diameter and 5 mm height), namely compressive strength and compressive stress, were tested by electronic universal testing machine (SUST IS09001, SUST, China). The compressing testing was performed at the speed of 1 mm/min and the maximum load of 10 kN. The value was recorded when the samples were compressed to 20% of their initial height. The Young's modulus was calculated according to the stress and strain. Five parallel tests were carried out for each sample.

2.3. Cell culturing and cell proliferation assay

Extracts of the samples were prepared as per ISO 10993-12. The samples were sterilized under UV for 30 min. Then the samples and the culture solution were put into a centrifuge tube, and the ratio of the surface area of the samples to the extracted liquid volume was 1.25 cm^2/mL. As the following step, the mixture was placed in an incubator for 72 h at 37 °C. Finally, the extracts were sealed and stored in 4 °C refrigerator for subsequent use.

Mouse pro-osteoblasts (MC3T3-E1, National Centre for Cell Science, Shanghai, China) were cultured in α-MEM medium (Beyotime, China) with 10% FBS (Gibco, America) and 2% double resistance (Trans-Gen Biotech, Beijing) solution in an incubator at 37 °C and 5% CO_2 atmosphere. The culture medium was changed every two days and passage of cells was executed when the cells growth reached 80% confluence.

Toxicity of the extracts on the MC3T3-E1 was evaluated. MC3T3-E1 cells were cultured with four different extracts, and the cell counting kit (CCK8, Beyotime, China) was used to assay the cell proliferative viability. Cell solution (5×10^4 cell/mL, 100 μL for each well) was added to 96-well plate and seeded for 12 h in the incubator. Subsequently the culture solution was replaced by the extracts and the culturing process was continued for 1 day, 2 days and 3 days (six parallel specimens for each sample). After culturing, the extracts in the plate were discarded and the plate was rinsed by PBS (HyClone, New Zealand). Then 100 μL of culture medium with 10% CCK8 solution was put into each well. After incubation for 2 h, the result was detected by enzyme mark instrument (Spectra Max 190, Molecular devices, America) operated at 450 nm wavelength.

2.4. Morphology characterization of the MC3T3-E1 cells on the filler surface

Morphology of the MC3T3-E1 cells attached on the fillers was characterized by SEM. The fillers were placed in 24-well plate and

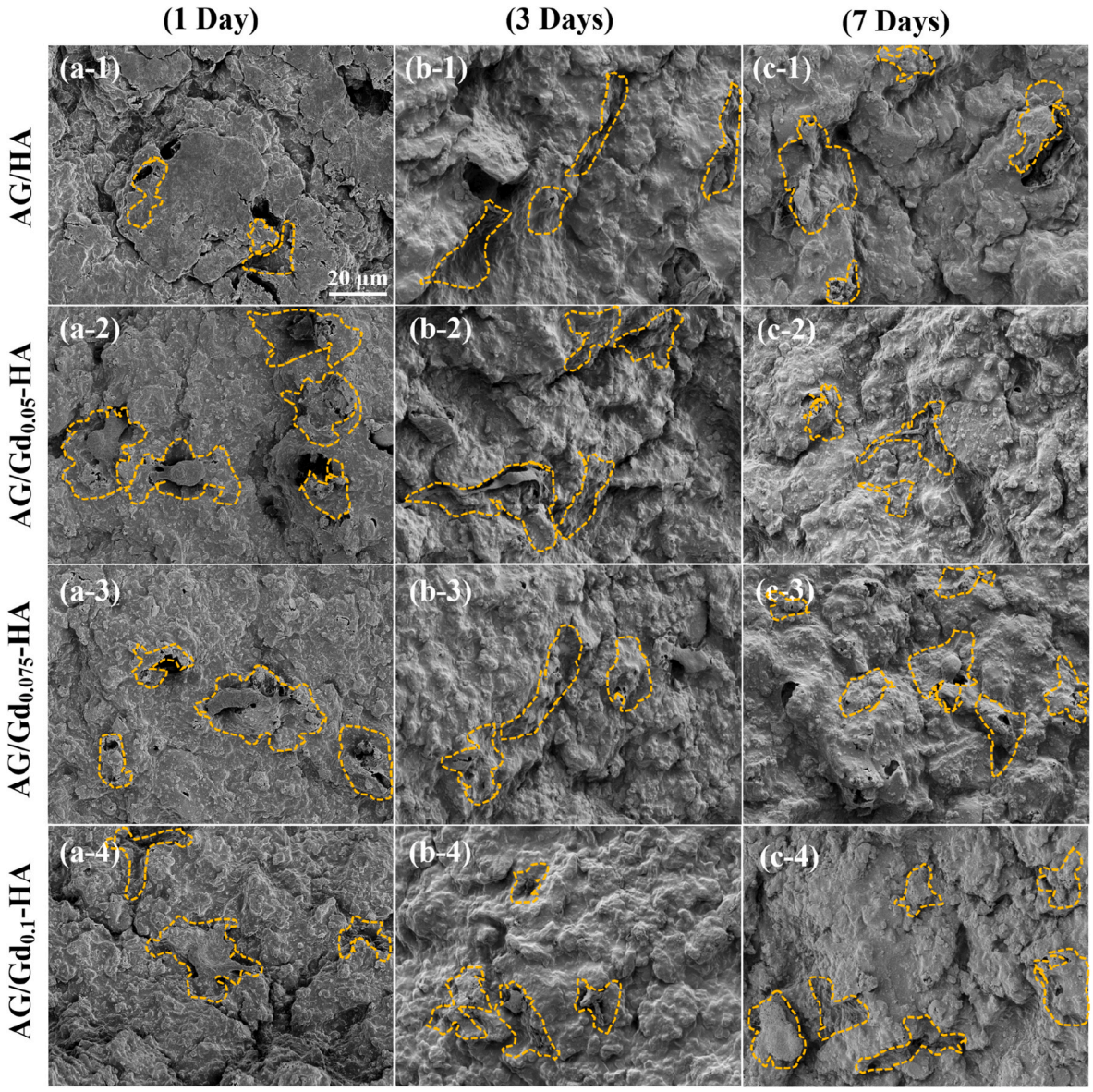

Fig. 8. Morphologies of the MC3T3-E1 cells proliferated on the fillers for 1 day (a), 3 days (b), and 7 days (c) (−1: the agarose/HA sample, −2: the agarose/$Gd_{0.05}$-HA sample, −3: the agarose/$Gd_{0.075}$-HA sample, −4: the agarose/$Gd_{0.1}$-HA sample, the orange circles point to the cells). The scale bar is 20 μm, AG stands for agarose.

sterilized under UV for 1 h. Then complete culture media for the cells were used to soak the fillers in the incubator for 2 h to make them fill with culture media. After incubated with culture media, the half-dried fillers were put into each well, and then 1 mL cells (5×10^4 cell/mL) were seeded to each well, and cultured in the incubator for 1 day, 3 days and 7 days. Prior to the SEM observation, the samples were fixed by 4% paraformaldehyde and dehydrated by 25%, 50%, 75%, and 90% ethanol for 5 min for once, then by 100% ethanol for 10 min for twice, respectively. Finally, the samples were vacuum dried at 37 °C and observed by SEM. In addition, the changes in chemical composition of the fillers after being soaked in culture medium for 1 day, 3 days, and 7 days were examined by ATR-FTIR, providing the in vitro degradation data of the fillers.

2.5. Osteogenic differentiation examination

Before Alizarin red staining, MC3T3-E1 cells were seeded at 5×10^4 cell/well in 24-well plates for 12 h, and then the culture medium was replaced by the four different extracts, which were refreshed every three days. Then the extracts were discarded and the samples were washed with PBS, and fixation fluid was used to fix cells for 20 min. Next, 100 μL dye was put into each well and covered cell for 30 min. Finally, the samples were washed with PBS and observed by inverted fluorescent microscope (DFC450C, Lecia, Germany). The experiment was performed at day 7 and day 14 to reveal the osteogenic differentiation of the samples.

2.6. Antibacterial properties of the agarose/Gd-HA fillers

To evaluate the antibacterial performances of the agarose/Gd-HA fillers, their sterilization against typical gram-positive bacteria (*Staphylococcus aureus*, *S. aureus*, ATCC6538) and typical gram-negative bacteria (*Escherichia coli*, *E. coli*, ATCC25922) was tested. For the testing, *S. aureus* and *E. coli* were cultured in TSB and LB medium in orbital shaker for 24 h at 37 °C and the agarose/Gd-HA samples were UV-sterilized for 1 h and placed in 24-well plate. Then 3 mL bacterial suspension with the concentration of 10^6 CFU/mL was added to each well containing UV-sterilized sample, and then incubated in orbital shaker at

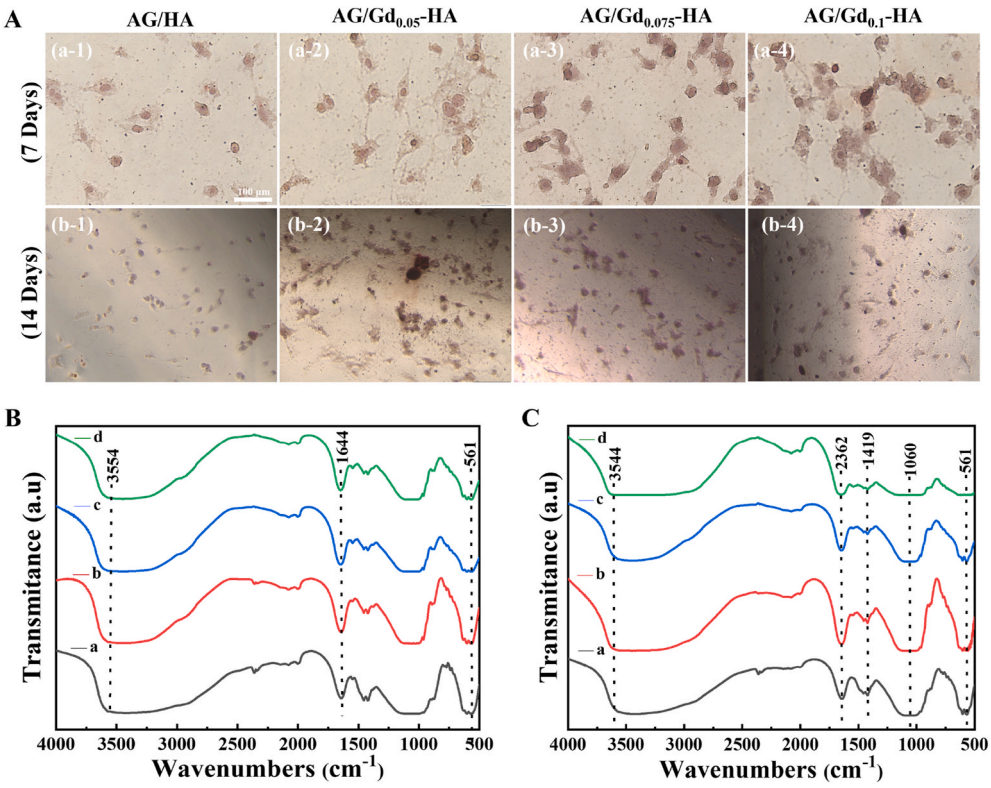

Fig. 9. Osteogenic activity testing of the samples (A), Alizarin red staining testing for (a) 7 days and (b) 14 days (−1: the agarose/HA sample, −2: the agarose/$Gd_{0.05}$-HA sample, −3: the agarose/$Gd_{0.075}$-HA sample, and −4: the agarose/$Gd_{0.1}$-HAsample, the scale bar is 100 μm) and ATR-FTIR evaluation of the agarose/HA sample (B) and the agarose/$Gd_{0.1}$-HA samples (C), the samples were soaked in culture medium for a:0 day, b:1 day, c:3 days, and d:7 days. AG stands for agarose.

37 °C. After 4 h, 12 h, 24 h, and 36 h, 100 μL suspension was taken out from each well, respectively, and the antibacterial rates were calculated using the spread plate counting method. Furthermore, the bacteria adhered on the sample surface at 24 h were observed by SEM to evaluate the anti-adherence performances of the samples.

2.7. Statistical analysis

At 95% and 99.5% confidence interval, statistical analyses were performed for all the experimental data (mean ± S.D) using SPSS 24.0 (SPSS Inc, Chicago, Illinois, USA). One-way analysis of variance (ANOVA) with last significant difference (LSD) test was conducted to assess the difference between different groups. P value of less than 0.05 and $P < 0.005$ were considered statistically significant.

3. Results and discussion

The changes of functional groups in the HA, $Gd_{0.1}$-HA, agarose, agarose/HA, and agarose/$Gd_{0.1}$-HA samples were examined by ATR-FTIR spectroscopy. The spectrum for HA shows the shoulders at 561 cm^{-1} and 604 cm^{-1}, suggesting the presence of PO_4^{3-} groups [39], the wide shoulder at 1060 cm^{-1} is assigned to P–O–P bonds, the weak shoulder at 1419 cm^{-1} is attributed to the combination of P═O bonds [41]. The peaks for OH^- group can be observed at 3459 cm^{-1} and 1644 cm^{-1}, and the wavenumber of 876 cm^{-1} refers to CO_3^{2-} groups [41]. Above results prove the successful synthesis of HA. For the $Gd_{0.1}$-HA sample, similar IR curve was seen with the curve for HA (Fig. 2 b versus Fig. 2 a), yet the shoulder at 1060 cm^{-1} is narrower and the intensity of the shoulder at 1419 cm^{-1} is lower than that of HA, suggesting successful doping of Gd into HA and reduced P–O chemical connection within HA crystals.

The IR spectrum of the agarose sample is shown in Fig. 2 c, the bands at 898 cm^{-1} and 931 cm^{-1} denote to the 3, 6-anydro-β-galactose and β-D-glucopyranose skeletal in agarose, the shoulders at 1378 cm^{-1}, 1644 cm^{-1} and 2904 cm^{-1} are attributed to C–O–C, C═O and C–H correlation acting bonds. The peaks at 2362 cm^{-1}, 1060 cm^{-1} and 3554 cm^{-1} suggest the interaction between O and H [42].

For the agarose/HA and the agarose/$Gd_{0.1}$-HA samples, their IR peaks at 604 cm^{-1} and 561 cm^{-1} refer to PO_4^{3-} groups in HA, and the intensity of the curve shoulders at 898 cm^{-1} and 931 cm^{-1} are remarkably weaker for the agarose/Gd-HA sample than that for the pure agarose, indicating that the original structure of agarose was already destroyed during its mixing processing with HA. The peak at 1060 cm^{-1} for agarose becomes widened, being likely due to the superimposed effect from the P–O–P bonds of HA and the O–H bonds in agarose. Moreover, it is noted that the peak at 3459 cm^{-1} for the curve of the agarose/$Gd_{0.1}$-HA disappeared, while the intensity of the peak at 3554 cm^{-1} for agarose increased. These are possibly due to the fact that the OH^- groups in the two components are similar. All the phenomena suggest that there are some chemical interactions between agarose and Gd-HA, and the addition of Gd-HA altered the physical structure of agarose. These structural changes would affect the biological behaviors of the samples.

To further detect the structural changes of the composite fillers, the doping effect of Gd in HA was characterized by XPS (Fig. 3). The $Gd_{0.1}$-HA sample was typically investigated, for which Ca 2p, P 2p, P 2s, O 1s and Gd 4d were detected. The binding energy of ~190 eV is assigned to P 2s that is formed in metal-P bonds, and the 132 eV belongs to P 2p that exists in P–O bonds in which P is tetrahedrally coordinated to O [37]. Peak separation spectra of Ca 2p and O 1s are shown in Fig. 3 b and Fig. 3 c. Ca 2p spectrum is divided into Ca 2p 3/2 and 1/2 peaks due to the spin orbit splitting. The peak at 345.104 eV represents Ca 2p 3/2, which forms a triangular net with Ca 2p 3/2 surrounding OH. Ca 2p 1/2 appears at 348.064 eV, which is parallel to *c* axis in a columnar structure like $CaCO_3$ [39]. For O 1s spectrum, the peak at 530.874 eV refers to O═P bonds, the peak at 529.098 eV delegates O–P/O-metal

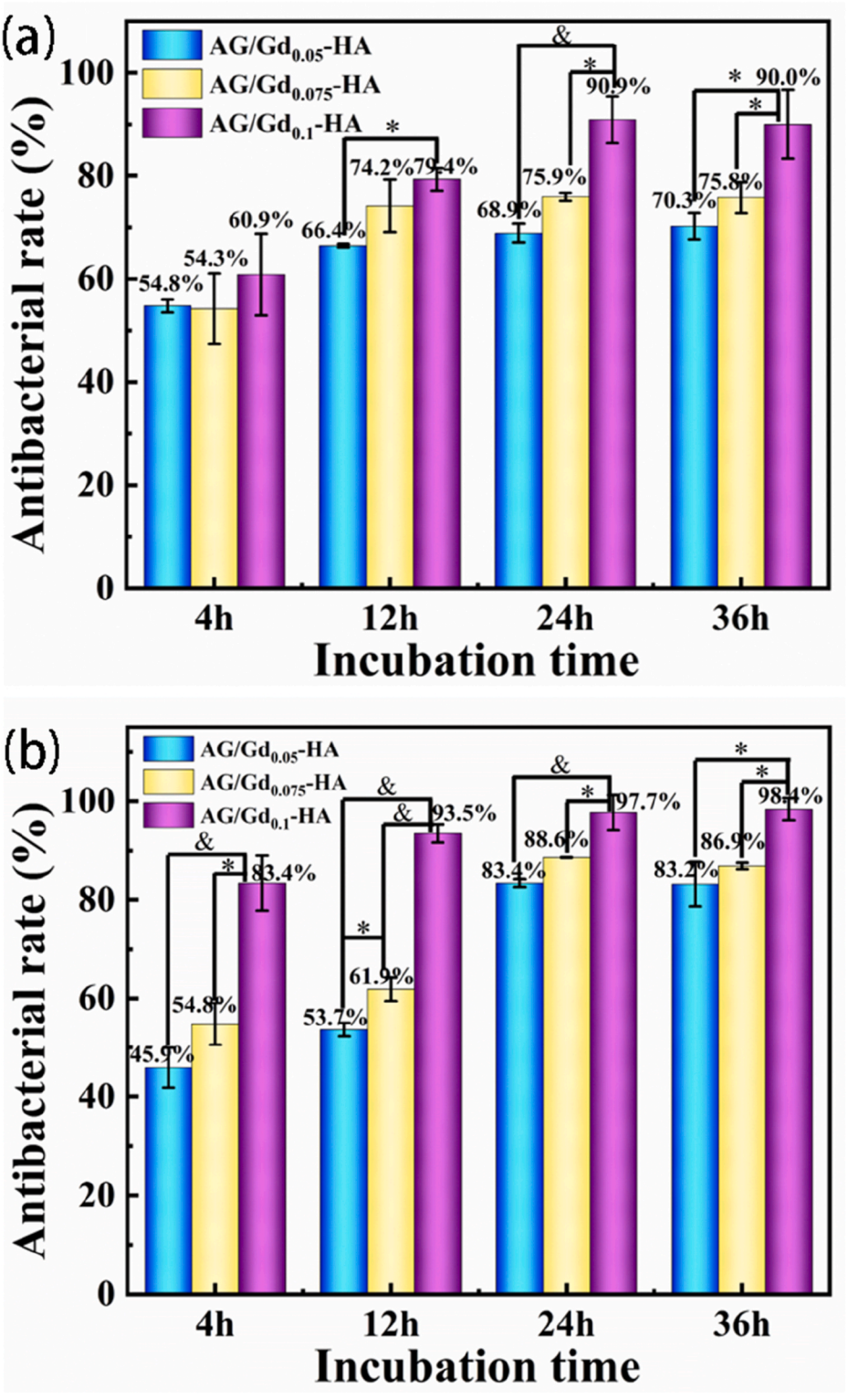

Fig. 10. Antibacterial rates of the agarose/Gd-HA fillers against bacteria *S. aureus* (a) and *E. coli* (b) after incubation for 4 h, 12 h, 24 h and 36 h. AG stands for agarose. $^{*}P < 0.05$, $^{\&}P < 0.005$.

(O–Ca/O–Gd) bonds which shows higher intensity than that in pure HA samples [39], indicating the formation of O–Gd bonds by the doping of Gd.

Gd 4d peaks are clearly seen (Fig. 3 d). Peaks at 151.004 eV, 146.651 eV and 141.364 eV all belong to the Gd–O bonds [40]. There is a high intensity peak at 131.1007 eV for Gd–P bond interaction, suggesting the predominant existing form of Gd after the doping into HA. Compared to the pure HA, remarkable differences in chemistry are seen for the Gd-HA. After the doping treatment, O 1s peak at 529.098 eV for O–P/O-metal bonds becomes stronger due to the addition of O–Gd bonds. In addition, O 1s region does not show OH bonds. P 2s appears in the scan spectrum, suggesting the binding of P with metal (Gd in this case). The clear appearance of Gd 4d indicates existence of Gd–O bonds and Gd–P bonds. All these information evidences successful doping of

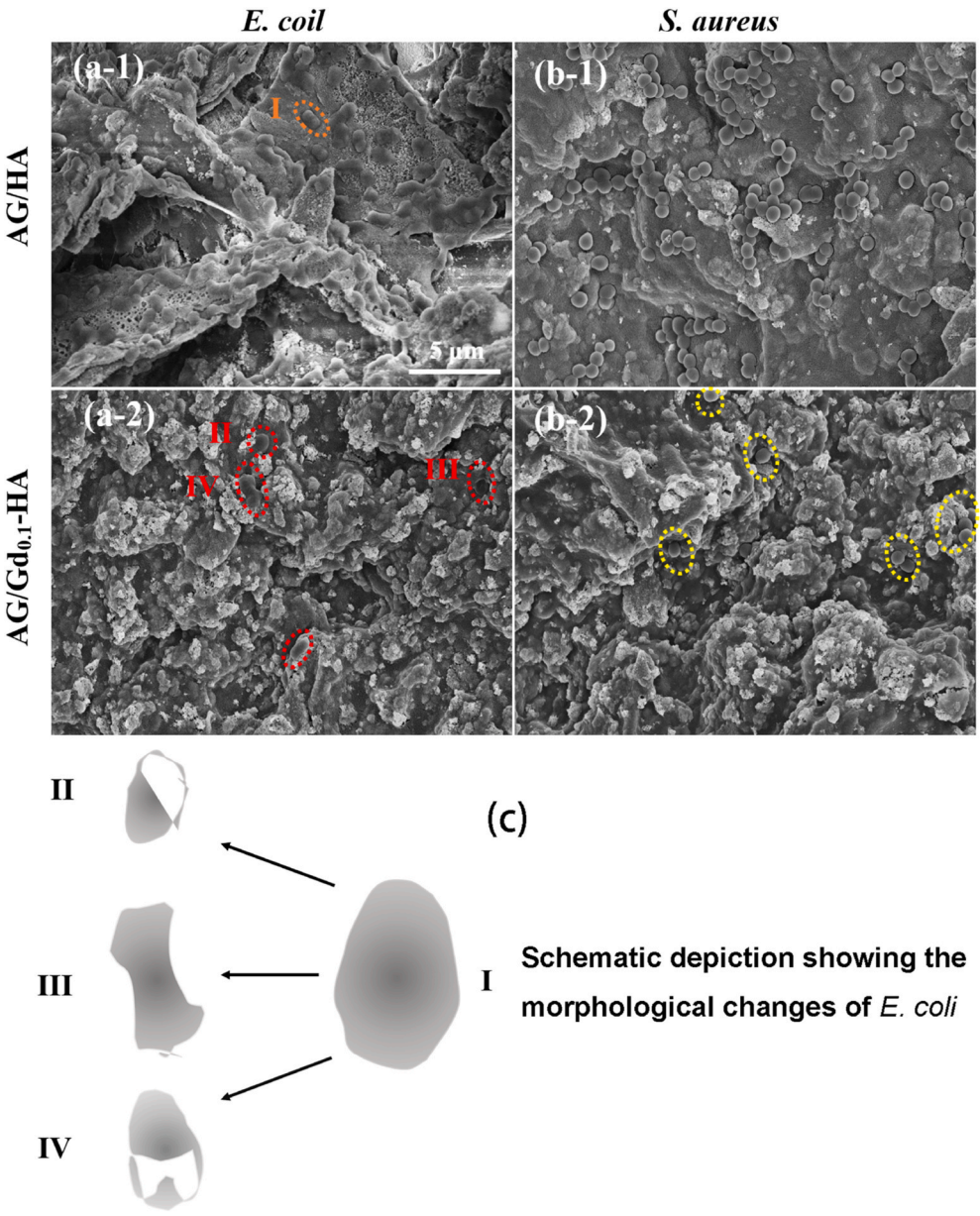

Fig. 11. SEM images showing the antibacterial effect of the Gd-containing agarose-HA composites, a-1: the agarose/HA sample after 24 h incubation in *E. coli* media, a-2: the agarose/HA sample after 24 h incubation in *S. aureus* media, b-1: the agarose/$Gd_{0.1}$-HA sample after 24 h incubation in *E. coli* media, b-2: the agarose/$Gd_{0.1}$-HA sample after 24 h incubation in *S. aureus* media (the red circles mark collapsed *E. coli* bacteria, the yellow circles mark destructed *S. aureus* bacteria), and c: schematic depiction showing morphology changes of *E. coli* bacterium after incubation in the media containing agarose/Gd-HA sample. The scale bar is 5 μm. AG stands for agarose.

Gd in HA structure, and the interaction and chemical bond between Gd and P further suggests the Gd-HA interstitial solid solution [39].

Morphological characterization of the agarose/HA sample showed an integrated and rugged surface (Fig. 4 a-1). Numerous nanoscale pores on the surface and a membranous surface layer can be clearly observed from the high magnification SEM image (Fig. 4 a-2). This integrated, rugged, and porous surface structure could promote the adhesion and growth of cells. Cross-sectional morphology of the freeze-dried sample exhibits a dense, rough, and multi-hole internal structure (Fig. 4 b-1, b-2), the size of the holes varies from nanoscale to microscale. This in turn suggests that the freeze-dried agarose/HA sample has hybrid mesoporous and micron-porous structure. This structure would benefit nutrients storing for cells and transfer of the metabolites produced by cells to the outside and therefore promotes the cells growth [9,10,15,16,43,44]. Moreover, this structure facilitates the occurrence of bone fusion and the formation of bone conduction nerve in bone tissue [45].

Swelling and water retention abilities are important performances for fillers, for excessive expansion ratio would cause stress on the tissues around the implant material and induce displacement of filling materials [46]. Low water-retention rate could decrease the ability of fillers to store nutrients [47], consequently deteriorating the growth of cells. The swelling ability testing showed that in PBS, the agarose sample has high expansion ratio (Fig. 5 a), it can quickly absorb PBS that is about 20 times of its weight, then the ratio kept stable at 15.5. The addition of HA in agarose sharply decreased the swelling ratio to ~3 and the time to adsorption equilibrium was extended to 50 min. The agarose/$Gd_{0.1}$-HA showed similar swelling property as the agarose/HA with the ratio of 2.6. Water retention ability testing of the samples showed that they underwent a typical dehydration process and reached equilibrium at 100 min (Fig. 5 b). The water retention of the agarose, the agarose/HA and the agarose/$Gd_{0.1}$-HA is 6.2%, 32.2% and 39%, respectively, indicating that the agarose/HA and the agarose/$Gd_{0.1}$-HA have lower de-swelling capacity than the pure agarose sample. These data further suggest the good water retention ability of the agarose/Gd-HA sample. HA enhanced the swelling and water retention properties of the agarose-based fillers for appropriate use in clinical surgery. Interestingly, it is noted that the incorporation of Gd in low dose did not remarkably impact the properties.

Mechanical properties of the samples were also examined. The value of compressive strength is 6827.33 N, 6741.19 N, 6739.01 N and 6786.19 N for the agarose/HA, the agarose/$Gd_{0.05}$-HA, the agarose/$Gd_{0.075}$-HA and the agarose/$Gd_{0.1}$-HA, respectively (Fig. 6 a). The value of compressive stress is correspondingly 86.26 MPa, 76.94 MPa, 79.73 MPa and 82.22 MPa. Compared to human bone with the compressive stress of 1–210 MPa [46], these fillers possess relatively sufficient mechanical strength for some applications in bone repair field. Additionally, the Young's modulus of the samples is 31.98 MPa, 28.82 MPa, 33.51 MPa, 33.16 MPa (Fig. 6 b), being comparable to the Young's modulus of cancellous human bone (0.8–1000 MPa [48]). It is realized that the doping of Gd has little influence on the mechanical properties of the samples, and the mechanical properties mainly depend on the crosslinking reactions within agarose chains, the intrinsic properties of HA, and the chemical interactions between agarose and Gd-HA.

Biocompatibility of the samples was evaluated by examining their cytotoxicity on MC3T3-E1 cells. Fig. 7 shows the CCK-8 testing results, the higher absorbance value suggests better cell proliferation and preferable biocompatibility of the samples. Compared with the agarose/HA, the doping dose of Gd from 5% to 10% showed nontoxicity to cells after 24 h culturing. With the extension of incubation time, the agarose/$Gd_{(0.05\text{-}0.1)}$-HA showed an effective activity of promoting cell proliferation, and the agarose/$Gd_{0.1}$-HA sample showed the best activity. Besides, it is noted that elongated incubation further enhanced the gaps in the absorbance values of the samples with/without the doping of Gd. This phenomenon evidences the result that the composite fillers promote cell proliferation. Strikingly, doping Gd into agarose/HA accelerated the cell growth, in the doping range of 5%–10%, more doped Gd gives rise to better promoting effect on cell growth. The agarose/$Gd_{0.1}$-HA filler exhibits the best promoting cell proliferation ability among the samples.

Fig. 8 shows the morphologies of the MC3T3-E1 cells adhered on the filler surfaces after incubation for 1 day, 3 days and 7 days. The doping of Gd did not affect the well spreading and adherence of the cells on the surfaces of the samples, which is consistent with the proliferation assay results (Fig. 7). Surprisingly, increased doping dose of Gd (from 5% to 10%), more adhered cells are seen on the sample surface and they show further stretched morphology. This phenomenon is in line with the CCK8 data that the doping of Gd in the agarose-HA has no toxicity on cells and can probably improve the biological properties.

The Alizarin red staining experiment was carried out to trace the calcium nodular formation in gross, which usually appears in the early stage of osteogenic differentiation. It seems clear that the redness appears based on the appearance of calcium nodules at day 7, indicating the generation of osteogenic differentiation. Over the culturing time, deepened and densified distribution of redness was formed in each group at day 21, which reflects the growth of calcium nodules and proves the development of osteogenic differentiation. Importantly, at the same culture time the redness was deeper, larger, and more for the composites with higher content of Gd (Fig. 9 A a-1, a-2, a-3, a-4). These results suggest favorable osteogenic activity of the newly developed agarose/Gd-HA filler, and the doping of Gd may promote the osteogenic activity of the fillers. In fact, it was reported that Gd^{3+} can promote the expression of Smad/5/8 and Runx-2 gene in osteoblasts, thereby activating Smad/Runx2 osteogenic signaling pathway and promoting osteogenic differentiation [49]. It seems the ionic state of Gd in the agarose/Gd-HA composites would influence their biological behaviors.

ATR-FITR spectroscopy detection further clarified the chemistry of the agarose/HA and agarose/$Gd_{0.1}$-HA fillers after being soaked in cultured medium (Fig. 9 B, C). For the agarose/HA sample (Fig. 9 B), weakened peaks at 3554 cm^{-1} (-OH/OH), 1644 cm^{-1} (C═O) and 561 cm^{-1} (PO_4^{3-}) are seen as the incubation time was prolonged, indicating continuous degradation of the agarose/HA in culture medium. Similarly, the spectrum of the agarose/$Gd_{0.1}$-HA sample shown in Fig. 9C illustrates the significantly weakened peaks at 3544 cm^{-1}, 2362 cm^{-1} (-OH/OH^-), 1419 cm^{-1} (P═O/Gd^{3+}-PO_4^{3-}), 1060 cm^{-1} (OH^-) and 561 cm^{-1} (PO_4^{3-}), further indicating enhanced degradation of the samples in the cultured media. This phenomenon nevertheless suggests that the doping of Gd likely increased the degradation of samples, and the degradation of agarose/$Gd_{0.1}$-HA would result in the increase in the concentration of Ca^{2+}, PO_4^{3-}, Gd^{3+} in culture medium, which in turn promotes the bioactivity of the samples [32].

The utmost purpose of this study was to construct the biological composites with antibacterial activities. Antibacterial examination using *S. aureus* and *E. coli* showed the antibacterial functions of the Gd-doped composites (Fig. 10). For the testing, the standard plate count (SPC) method [38] was employed to estimate the sterilization rate of the fillers to the surrounding suspended bacteria. It is noted that the agarose/HA sample has no antibacterial activity. The rate of the sterilization against *S. aureus* after incaution of the samples in bacteria suspension for 4 h is 54.8%, 54.3% and 60.9% for the agarose/$Gd_{0.05}$-HA, the agarose/$Gd_{0.075}$-HA and the agarose/$Gd_{0.1}$-HA samples, respectively (Fig. 10 a). No significant differences are seen among the samples. The antibacterial rates increased to66.4%, 74.2% and 79.4% respectively after 12 h incubation. Further incubation to 24 h and 36 h resulted in different antibacterial responses of the different samples, that is, the antibacterial rate of the agarose/$Gd_{0.05}$-HA and the agarose/$Gd_{0.075}$-HA samples is 68.9% and 75.9%, respectively, which kept almost unchanged as compared to the data obtained after 12 h incubation. It is surprisingly noted that the antibacterial rate of the agarose/$Gd_{0.1}$-HA after 24 h incubation increased to 90.9%, and it keeps stable after 36 h incubation (90.0%). Obviously, the dose of Gd in the composites plays important role in regulating their antibacterial performances. For the *E. coli* bacteria, similar trend was revealed that increased dose of Gd and elongated incubation brought about augmented antibacterial rate (Fig. 10 b). The antibacterial rate keeps stable after incubation time over 24 h, and it reached 83.2%, 86.9% and 98.4% for the agarose/$Gd_{0.05}$-HA, the agarose/$Gd_{0.075}$-HA and the agarose/$Gd_{0.1}$-HA samples after 36 h incubation. The agarose/$Gd_{0.1}$-HA sample showed the best antibacterial activity against both *S. aureus* and *E. coli*. The low dose addition of Gd already offers significant antibacterial activity for the biocompatible composites.

Anti-microbial activity of the rare earth element Gd has been investigated [50–52]. Its antibacterial activity mainly involves Gd^{3+}. Gd^{3+} can replace Ca^{2+} to participate in the physiological activities of bacteria to decrease the biological activity and cause bacteria apoptosis [50]. In addition, Gd^{3+} can destroy the wall structure of bacteria through electric field adsorption, which makes the permeability of bacterial cell membrane changed and finally results in bacterial death [51]. Furthermore, Gd^{3+} is able to combine with other functional groups in bacteria, those groups are capable of destroying the normal metabolic activity of bacteria [52]. In this case, adherence of the bacteria on the surfaces of the agarose/HA and the agarose/$Gd_{0.1}$-HA fillers are clearly seen after the incubation for 24 h (Fig. 11). It was found that the 24 h incubation already resulted in a stable antibacterial rate of the Gd-containing fillers (Fig. 10). Numerous *E. coli* bacteria with healthy bacterial morphology can be observed on the Gd-free agarose/HA surface (Fig. 11 a-1), while sharply decreased number of the bacteria (as marked by the red circles) is seen on the agarose/$Gd_{0.1}$-HA surface (Fig. 11 a-2). Destructive morphology is clear for those bacteria adhered on the Gd-containing sample surface, indicating the antibacterial function of the sample. Remarkable morphology changes of *E. coil* are realized (Fig. 11 a-2), and these changes were schematically depicted (Fig. 11 c). Similarly, *S. aureus* bacteria with normal morphology are seen on the surface of the Gd-free agarose/HA filler (Fig. 11 b-1), while the bacteria (as marked by the yellow circles) are rarely seen on the agarose/$Gd_{0.1}$-HA surface (Fig. 11 b-2), the morphology of *S. aureus* shows minor differences on the different samples. These results are consistent with the standard plate count testing data that the low-dose doping of Gd offers the agarose-HA composites distinct antibacterial properties for both *S. aureus* and *E. coli*. The biocompatible agarose/$Gd_{0.1}$-HA filler has the potential to prohibit or avoid post-surgery bacterial infection.

4. Conclusions

Gd-doped hydroxyapatite powder with antibacterial activities was prepared using chemical precipitation method, and Gd was doped into HA crystal and the main existing connection form was Gd–P. Agarose/Gd-HA fillers with porous three-dimensional structures were fabricated by physical mixing and freeze-drying. The fillers possess competent mechanical properties, and the swelling and de-swelling experiments showed the potential of the agarose/Gd-HA fillers as bone implantation material. The cell culturing testing further evidenced the favorable biological and osteogenic activity of the newly developed composites, and the doping of Gd with the content of 5%–10% promoted the proliferation and osteogenesis of the cells. The antibacterial testing of the Gd-containing composites showed clear evidence that the agarose-HA was endowed by Gd with the antibacterial ability for both gram-positive *S. aureus* and gram-negative *E. coli*. The agarose/$Gd_{0.1}$-HA sample showed the best antibacterial effect. The design of and fabrication technical route for the Gd-doped agarose-HA composites with synergistic biocompatibility and antibacterial activity would shed light on developing new bone defects fillers for bone repair applications.

Declaration of competing interest

The authors declare that they have no known competing financial interests or personal relationships that could have appeared to influence the work reported in this paper.

Acknowledgements

This research was supported by National Natural Science Foundation of China (grant # 52071329), Zhejiang Provincial Natural Science Foundation of China (grant # LY18C100003), K. C. Wong Education Foundation (grant # GJTD-2019-13), The Youth Innovation Promotion Association of the Chinese Academy of Sciences, China (grant # 2020299), and Innovation 2025 Major Special Program of Ningbo, China.

References

[1] T.D. Rachner, S. Khosl, L.C. Hofbauer, Osteoporosis: now and the future, Lancet 377 (2011) 1276–1287, https://doi.org/10.1016/S0140-6736(10)62349-5.
[2] M. Tamaddon, L. Wang, Z.Y. Liu, C.Z. Liu, Osteochondral tissue repair in osteoarthritic joints: clinical challenges and opportunities in tissue engineering, Biodes. Manuf. 1 (2018) 101–114, https://doi.org/10.1007/s42242-018-0015-0.
[3] T. Matsuo, K. Kita, M.A.E.T. Mae, Y. Yasukazu, M. Satoshi, Y. Hideki, N. Ken, Bone substitutes and implantation depths for subchondral bone repair in osteochondral defects of porcine knee joints, Knee Surg. Sports Traumatol. Arthrosc. 23 (2015) 1401–1409, https://doi.org/10.1007/s00167-014-2853-4.
[4] S.V. Dorozhkin, Calcium orthophosphate deposits: preparation, properties and biomedical applications, Mater. Sci. Eng. C 55 (2015) 272–326, https://doi.org/10.1016/j.msec.2015.05.033.
[5] D. Puppi, F. Chiellini, A.M. Piras, E. Chiellini, Polymeric materials for bone and cartilage repair, Prog. Polym. Sci. 35 (2010) 403–440, https://doi.org/10.1016/j.progpolymsci.2010.01.006.
[6] Y.L. Zhu, Z.J. Ma, L.Z. Kong, Y.H. He, H.F. Chan, H.Y. Li, Modulation of macrophages by bioactive glass/sodium alginate hydrogel is crucial in skin regeneration enhancement, Biomaterials 256 (2020) 120216, https://doi.org/10.1016/j.biomaterials.2020.120216.
[7] H.R. Lin, Y.J. Yeh, Porous alginate/hydroxyapatite composite fillers for bone tissue engineering: preparation, characterization, and in vitro studies, J. Biomed. Mater. Res. B 71 (2004) 52–65, https://doi.org/10.1002/jbm.b.30065.
[8] H. Samadian, H. Mobasheri, M. Azami, R. Faridi-Majidi, Osteoconductive and electroactive carbon nanofibers/hydroxyapatite nanocomposite tailored for bone tissue engineering: in vitro and in vivo studies, Sci. Rep. 10 (2020) 14853, https://doi.org/10.1038/s41598-020-71455-3.
[9] N. Sykaras, , DDS, A.M. Lacopino, , DMD, V.A. Marker, R.G. Triplett, , DSS, R. D. Woody, DDS, Implant materials, designs, and surface topographies: their effect on osseointegration. A literature review, Int. J. Oral Maxillofac. Implants 15 (2000) 16, https://doi.org/10.1046/j.1365-2591.2000.00364.x.
[10] T. Su, M.Y. Zhang, Q.K. Zeng, W.H. Pan, Y.J. Huang, Y. Qian, W. Dong, X.L. Qi, J. L. Shen, Mussel-inspired agarose hydrogel fillers for skin tissue engineering, Bioact. Mater. 6 (2021) 579–588, https://doi.org/10.1016/j.bioactmat.2020.09.004.
[11] M. Jafari, Z. Paknejad, M.R. Rad, S.R. Motamedian, M.J. Eghbal, N. Nadjmi, A. Khojasteh, Polymeric scaffolds in tissue engineering: a literature review, J. Biomed. Mater. Res. B 105 (2017) 431–459, https://doi.org/10.1002/jbm.b.33547.
[12] F. Croisier, C. Jérôme, Chitosan-based biomaterials for tissue engineering, Eur. Polym. J. 49 (2013) 780–792, https://doi.org/10.1016/j.eurpolymj.2012.12.009.
[13] P. Zarrintaj, S. Manouchehri, Z. Ahmadi, R.S. Mohammad, U. Aleksandra, M., K. David, L.,M. Masoud, Agarose-based biomaterials for tissue engineering, Carbohydr, Polym 187 (2018) 66–84, https://doi.org/10.1016/j.carbpol.2018.01.060.
[14] C.T. Buckley, S.D. Thorpe, F.J. O'brien, A.J. Robinson, D.J. Kelly, The effect of concentration, thermal history and cell seeding density on the initial mechanical properties of agarose hydrogels, J. Mech. Behav. Biomed. Mater. 2 (2009) 512–521, https://doi.org/10.1016/j.jmbbm.2008.12.007.
[15] G. Zhong, J. Yao, X. Huang, Y.X. Luo, M. Wang, J.Y. Han, F. Chen, Y. Yu, Injectable ECM hydrogel for delivery of BMSCs enabled full-thickness meniscus repair in an orthotopic rat model, Bioact. Mater. 5 (2020) 871–879, https://doi.org/10.1016/j.bioactmat.2020.06.008.
[16] J.J. Xu, G.Y. Wang, Y.F. Wu, X.Y. Ren, G.H. Gao, Ultrastretchable wearable strain and pressure sensors based on adhesive, tough, and self-healing hydrogels for human motion monitoring, ACS Appl. Mater. Interfaces 11 (2019) 25613–25623, https://doi.org/10.1021/acsami.9b08369.
[17] W.Y. Gu, H. Yao, C.Y. Huang, H.S. Cheung, New insight into deformation-dependent hydraulic permeability of gels and cartilage, and dynamic behavior of agarose gels in confined compression, J. Biomech. 36 (2003) 593–598, https://doi.org/10.1016/S0021-9290(02)00437-2.
[18] P. Kazimierczak, M. Koziol, A. Przekora, The chitosan/agarose/nanoHA bone scaffold-induced M2 macrophage polarization and its effect on osteogenic differentiation in vitro, Int. J. Mol. Sci. 22 (2021) 1–14, https://doi.org/10.3390/ijms22031109.
[19] Y.P. Liang, X. Zhao, T.L. Hu, B.J. Chen, Z.H. Yin, P.X. Ma, B.L. Guo, Adhesive hhemostatic conducting injectable composite hydrogels with sustained drug release and photothermal antibacterial activity to promote full-thickness skin regeneration during wound healing, Small 15 (2019) 1900046, https://doi.org/10.1002/smll.201900046.
[20] H. Ghasemzadeh, S. Afraz, M. Moradi, S. Hassanpour, Antimicrobial chitosan-agarose full polysaccharide silver nanocomposite films, Int. J. Biol. Macromol. 179 (2021) 532–541, https://doi.org/10.1016/j.ijbiomac.2021.02.192.
[21] P. Kazimierczak, A. Benko, M. Nocun, A. Przekora, Novel chitosan/agarose/hydroxyapatite nanocomposite scaffold for bone tissue engineering applications: comprehensive evaluation of biocompatibility and osteoinductivity with the use of osteoblasts and mesenchymal stem cells, Int. J. Nanomed. 14 (2019) 6615–6630, https://doi.org/10.2147/IJN.S217245.
[22] D.D. Deligianni, N.D. Katsala, P.G. Koutsoukos, Y.F. Missirlis, Effect of surface roughness of hydroxyapatite on human bone marrow cell adhesion, proliferation, di!erentiation and detachment strength, Biomaterials 22 (2001), https://doi.org/10.1016/S0142-9612(00)00174-5, 87-76.
[23] R. Donate, M. Monzón, M.E. Alemán-Domínguez, Z. Ortega, Enzymatic degradation study of PLA-based composite fillers, Rev. Adv. Mater. Sci. 59 (2020) 170–175, https://doi.org/10.1515/rams-2020-0005.
[24] X. Liu, C.Y. Bao, H.H.K. Xu, J. Pan, J. Hu, P. Wang, E. Luo, Osteoprotegerin gene-modified BMSCs with hydroxyapatite scaffold for treating critical-sized mandibular defects in ovariectomized osteoporotic rats, Acta Biomater. 42 (2016) 378–388, https://doi.org/10.1016/j.actbio.2016.06.019.
[25] H. Kang, C. Wen, Y. Hwang, Y.V. Shih, M. Kar, S.W. Seo, S. Varghese, Biomineralized matrix-assisted osteogenic differentiation of human embryonic stem cells, J. Mater. Chem. B 2 (2014) 5676–5688, https://doi.org/10.1039/c4tb00714j.
[26] M. Tsukanaka, S. Fujibayashi, B. Otsuki, M. Takemato, S. Matsuda, Osteoinductive potential of highly purified porous beta-TCP in mice, J. Mater. Sci. Mater. Med. 26 (2015) 132, https://doi.org/10.1007/s10856-015-5469-4.
[27] H. Zhou, J. Lee, Nanoscale hydroxyapatite particles for bone tissue engineering, Acta Biomater. 7 (2011) 2769–2781, https://doi.org/10.1016/j.actbio.2011.03.019.
[28] A. Fihri, C. Len, R.S. Varma, A. Solhy, Hydroxyapatite: a review of syntheses, structure and applications in heterogeneous catalysis, Coord. Chem. Rev. 347 (2017) 48–76, https://doi.org/10.1016/j.ccr.2017.06.009.
[29] Y. Yang, K. Serpersu, W. He, S.R. Paital, N.B. Dahotre, Osteoblast interaction with laser cladded HA and SiO_2-HA coatings on Ti-6Al-4V, Mater. Sci. Eng. C 31 (2011) 1643–1652, https://doi.org/10.1016/j.msec.2011.07.009.
[30] N. Vargas-Becerril, D.A. Sánchez-Téllez, L. Zarazúa-Villalobos, D. M. GonzálezGarcía, M.A. Álvarez-Pérez, C. León-Escobedo, L. Téllez-Jurado, Structure of biomimetic apatite grown on hydroxyapatite (HA), Ceram. Int. 46 (2020) 28806–28813, https://doi.org/10.1016/j.ceramint.2020.08.044.
[31] Ž. Radovanovic, B. Jokic, D. Veljovic, S. Dimitrijevic, V. Kojic, R. Petrovic, D. Janackovic, Antimicrobial activity and biocompatibility of Ag^{+}- and Cu^{2+}-doped biphasic hydroxyapatite/α-tricalcium phosphate obtained from hydrothermally synthesized Ag^{+}- and Cu^{2+}-doped hydroxyapatite, Appl. Surf. Sci. 307 (2014) 513–519, https://doi.org/10.1016/j.apsusc.2014.04.066.
[32] X. Wu, J. Li, L. Wang, D. Huang, Y. Zuo, Y. Li, The release properties of silver ions from Ag-nHA/TiO_2/PA66 antimicrobial composite fillers, Biomed. Mater. 5 (2010), 044105, https://doi.org/10.1088/1748-6041/5/4/044105.
[33] S. Balakrishnan, V.P. Padmanabhan, R. Kulandaivelu, S.N. Nellaiappan TS, S. Sagadevan, S. Paiman, F. Mohammad, H.A. Al-Lohedan, P.K. Obulapuram, W. C. Oh, Influence of iron doping towards the physicochemical and biological characteristics of hydroxyapatite, Ceram. Int. 47 (2021) 5061–5070, https://doi.org/10.1016/j.ceramint.2020.10.084.

[34] S. Zaichick, V. Zaichick, V. Karandashev, S. Nosenko, Accumulation of rare earth elements in human bone within the lifespan, Metallomics 3 (2011) 186–194, https://doi.org/10.1039/c0mt00069h.
[35] T. Wakabayashi, A. Ymamoto, A. Kazaana, Y. Nakano, Y. Nojiri, M. Kashiwazaki, Antibacterial, antifungal and nematicidal activities of rare earth ions, Biol. Trace Elem. Res. 174 (2016) 464–470, https://doi.org/10.1007/s12011-016-0727-y.
[36] C. Huang, Y. Huang, N. Tian, Y. Tong, R. Yin, Preparation and characterization of gelatin/cerium(III) film, J. Rare Earths 28 (2010) 756–759, https://doi.org/10.1016/S1002-0721(09)60195-2.
[37] P.P. Mokoena, I.M. Nagpure, V. Kumar, R.E. Kroon, E.J. Olivier, J.H. Neethling, H. C. Swart, O.M. Ntwaeaborwa, Enhanced UVB emission and analysis of chemical states of $Ca_5(PO_4)_3OH$: Gd^{3+}, Pr^{3+} phosphor prepared by co-precipitation, J. Phys. Chem. Solid. 75 (2014) 998–1003, https://doi.org/10.1016/j.jpcs.2014.04.015.
[38] C. Yang, J. Liu, Q. Ren, Y. Liu, P. Zhou, H. Li, Development of novel thermal sprayed hydroxyapatite-rare earth (HA-Re) coatings for potential antimicrobial applications in orthopedics, J. Therm. Spray Technol. 30 (2021) 886–997, https://doi.org/10.1007/s11666-021-01154-6.
[39] M.F. Cipreste, A.M. Peres, A.A.C. Cotta, F.H. Aragon, A.M. Antunes, A.S. Leal, W.A. A. Macedo, E.M.B. Sousa, Synthesis and characterization of ^{159}Gd-doped hydroxyapatite nanorods for bioapplications as theranostic systems, Mater. Chem. Phys. 181 (2016) 301–311, https://doi.org/10.1016/j.matchemphys.2016.06.063.
[40] K. Saranya, S. Bhuvaneswari, S. Chatterjee, N. Rajendran, Biocompatible gadolinium-coated magnesium alloy for biomedical applications, J. Mater. Sci. 55 (2020) 11582–11596, https://doi.org/10.1007/s10853-020-04742-z.
[41] P. Kazimierczak, A. Benko, K. Palka, C. Canal, D. Kolodynska, A. Przekora, Novel synthesis method combining a foaming agent with freeze-drying to obtain hybrid highly macroporous bone scaffolds, J. Mater. Sci. Technol. 43 (2020) 52–63, https://doi.org/10.1016/j.jmst.2020.01.006.
[42] X. Qi, T. Su, X. Tong, W. Xiong, Q. Zeng, Y. Qian, Z. Zhou, X. Wu, Z. Li, L. Shen, X. He, C. Xu, M. Chen, Y. Li, J. Shen, Facile formation of salecan/agarose hydrogels with tunable structural properties for cell culture, Carbohydr. Polym. 224 (2019) 115208, https://doi.org/10.1016/j.carbpol.2019.115208.
[43] B. Abar, A. A Alonso-Calleja, A. Kelly, C. Kelly, K. Gall, J.L. West, 3D Printing of High-Strength, Porous, Elastomeric Structures to Promote Tissue Integration of Implants, https://doi.org/10.1002/jbm.a.37006.
[44] A. Marrella, A. Lagazzo, E. Dellacasa, C. Pasaquini, E. Finocchio, F. Barberis, L. Pastorino, S. Scaglione, 3D porous gelatin/PVA hydrogel as meniscus substitute using alginate micro-particles as porogens, Polymers 10 (2018) 380, https://doi.org/10.3390/polym10040380.
[45] A.C. Jones, C.H. Arns, A.P. Sheppard, D.W. Hutmacher, B.K. Milthorpe, M. A. Knackstedt, Assessment of bone ingrowth into porous biomaterials using MICRO-CT, Biomaterials 28 (2007) 2491–2504, https://doi.org/10.1016/j.biomaterials.2007.01.046.
[46] F. Yu, T.R. Cui, C.F. Yang, X.H. Dai, J. Ma, k-Carrageenan/Sodium alginate double-network hydrogel with enhanced mechanical properties, anti-swelling, and adsorption capacity, Chemosphere 237 (2019) 124417, https://doi.org/10.1016/j.chemosphere.2019.124417.
[47] M.H. Zhang, S.Y. Chen, N. Sheng, B.X. Wang, J.J. Yao, Z.T. Wu, H.P. Wang, A strategy of tailoring polymorphs and nanostructures to construct self-reinforced nonswelling high-strength bacterial cellulose hydrogels, Nanoscale 11 (2019) 15347, https://doi.org/10.1039/c9nr04462k.
[48] R. Adamski, D. Siuta, Mechanical, structural, and biological properties of chitosan/hydroxyapatite/silica composites for bone tissue engineering, Molecules 26 (2021), https://doi.org/10.3390/molecules26071976, 1976.
[49] P.-P. Zhao, H.-R. Hu, J.-Y. Liu, Q.-F. Ke, X.-Y. Peng, H. Ding, Y.-P. Guo, Gadolinium phosphate/chitosan scaffolds promote new bone regeneration via Smad/Runx2 pathway, Chem. Eng. J. 359 (2019) 1120–1129, https://doi.org/10.1016/j.cej.2018.11.071.
[50] P. Liu, Y. Liu, Z. Lu, J. Zhu, J. Dong, D. Pang, P. Shen, S. Qu, Study on biological effect of La^{3+} on Escherichia coli by atomic force microscopy, J. Inorg. Biochem. 98 (2004) 68–72, https://doi.org/10.1016/j.jinorgbio.2003.08.012.
[51] J.L. Wei, D.Y. Huang, Y.C. Chen, Using gadolinium ions as affinity probes to selectively enrich and magnetically isolate bacteria from complex samplesm, Anal. Chim. Acta 1113 (2020) 18–25, https://doi.org/10.1016/j.aca.2020.03.046.
[52] M. Yon, S. Gineste, G. Parigi, B. Lonetti, L. Gibot, D.R. Talham, J.-D. Marty, C. Mingotaud, Hybrid polymeric nanostructures stabilized by zirconium and gadolinium ions for use as magnetic resonance imaging contrast agents, ACS Appl. Nano Mater. 4 (2021) 4974–4982, https://doi.org/10.1021/acsanm.1c00495.